Eur. Phys. J. B **14**, 1–10 (2000)

THE EUROPEAN PHYSICAL JOURNAL B

EDP Sciences

Superconducting and magnetic properties of $Nb/Pd_{1-x}Fe_x/Nb$ triple layers

M. Schöck, C. Sürgers[a], and H.v. Löhneysen

Physikalisches Institut, Universität Karlsruhe, 76128 Karlsruhe, Germany

Received 15 December 1998 and Received in final form 26 April 1999

Abstract. The superconducting and magnetic properties of $Nb/Pd_{1-x}Fe_x/Nb$ triple layers with constant Nb layer thickness $d_{Nb} = 200$ Å and different interlayer thicknesses 3 Å $\leq d_{PdFe} \leq 80$ Å are investigated. The thickness dependence of the magnetization and of the superconducting transition temperature shows that for small iron concentration x the $Pd_{1-x}Fe_x$ layer is likely to be in the paramagnetic state for very thin films whereas ferromagnetic order is established for $x \geq 0.13$. The parallel critical field $B_{c2\parallel}(T)$ exhibits a transition from two-dimensional (2D) behavior where the Nb films are coupled across the interlayer, towards a 2D behavior of decoupled Nb films with increasing d_{PdFe} and/or x. This transition allows a determination of the penetration depth ξ_F of Cooper pairs into the $Pd_{1-x}Fe_x$ layer as a function of x. For samples with a ferromagnetic interlayer ξ_F is found to be independent of x.

PACS. 74.50.+r Proximity effects, weak links, tunneling phenomena, and Josephson effects – 74.80.Dm Superconducting layer structures: superlattices, heterojunctions, and multilayers – 75.70.Ak Magnetic properties of monolayers and thin films

1 Introduction

The proximity effect of a superconductor (S) in contact with a ferromagnet (F) has attracted considerable new interest, since an oscillatory behavior of the Cooper pair amplitude in the ferromagnet was predicted theoretically in S/F multilayers [1,2]. Due to the exchange field in the ferromagnet, the pair-breaking parameter is complex and causes a spacial modulation of the superconducting order parameter in the ferromagnetic interlayer. For certain thicknesses d_F of the ferromagnetic layer the phase of the order parameter changes by $\Delta\phi = \pi$ across the barrier (so-called π-junction [3]) which gives rise to an enhanced transition temperature T_c. This, for instance, should show up in a nonmonotonic dependence of $T_c(d_F)$. Further theoretical work has shown that these anomalies should also occur in S/F bilayers [4,5].

Several experimental studies have been performed to search for the appearance of π-coupling in S/F multilayers and triple layers [6–12]. However, up to now none of the investigations have revealed unambiguously a nonmonotonic behavior due to a π-coupling mechanism. Although the measurements on sputtered Nb/Gd multilayers and triple layers have been interpreted in terms of this mechanism [10,11], the loss of ferromagnetic order at thin interlayer thicknesses [7] or a magnetically "dead" interface region can also result in a nonmonotonic behavior of $T_c(d_F)$ [13]. Furthermore, the magnitude of the electron mean-free path l in S and F, the interface transparency, and spin-orbit scattering must be taken into account [4,5,14].

A prominent parameter which enters all of the present theories is the characteristic complex decay constant k_F describing the decay of the pair amplitude F_F in the F layer along the surface normal x, *i.e.* $F_F \propto \exp(-k_F x)$. The real part of k_F defines the exponential decay of the envelope of F_F, *i.e.* the penetration depth of Cooper pairs in the F layer, whereas the imaginary part defines oscillations of F_F. In the theory of Radović *et al.* these two length scales turn out to be identical, $(\mathrm{Im}\, k_F)^{-1} = (\mathrm{Re}\, k_F)^{-1} = \xi_F/2$, with the characteristic length ξ_F defined as $\xi_F = \sqrt{4\hbar D_F/I}$. D_F is the electronic diffusion constant in F and $2I$ is the splitting of the spin-up and spin-down conduction bands by the exchange interaction [2]. However, the penetration depth and the oscillation period of F_F can be different for small electron mean free paths and strong spin-orbit scattering [4,5].

In recent experiments which have been mainly discussed in frame of the theory by Radović *et al.* the length ξ_F often serves as an adjustable parameter. In this paper, we will focus on the upper critical field of triple layers and show that ξ_F can be determined from a transition in the T dependence of the parallel upper critical field of $Nb/Pd_{1-x}Fe_x/Nb$ triple layers rather than use it as a free parameter whose value depends on the theoretical model

[a] e-mail: christoph.suergers@physik.uni-karlsruhe.de

employed. This transition from two-dimensional (2D) behavior of the whole triple layer to 2D behavior of each Nb film individually, can only be observed for a thickness d_F smaller than a critical thickness d_c, which will be identified as ξ_F, see below. The influence of different ferromagnetic materials on the superconducting properties of S/F multilayers has been studied previously by Koorevaar *et al.* [9] where the emphasis was put on the critical thickness of the superconducting layers which are decoupled by thick ferromagnetic interlayers. In contrast, the present work focuses on the influence of the ferromagnetic layer thickness in S/F/S triple layers with superconducting layers of constant thickness. We will furthermore show that the analysis of the superconducting properties allows access to the magnetic properties in thin ferromagnetic films.

The ferromagnetic behavior of $Pd_{1-x}Fe_x$ alloys has been studied in great detail, in particular the Pd-rich alloys [15]. In $Pd_{1-x}Fe_x$, the Curie temperature T_{Curie} can be changed over a wide range of concentration x. For small x, the polarization of the Pd conduction band around each localized Fe moment gives rise to a "giant moment" of 13–16 μ_B per Fe impurity [16]. In addition, the Fe–Pd exchange interaction leads to an indirect ferromagnetic Fe–Fe interaction. In bulk alloys, ferromagnetism persists down to a concentration of about $x \approx 10^{-4}$ (Ref. [17]) and T_{Curie} increases monotonically with increasing x. Furthermore, with increasing x the electronic structure gradually changes from a localized to a more itinerant behavior [23] and direct Fe–Fe interactions become important. In the present work we use the large variability in T_{Curie} and interaction strength with x to tune the S/F coupling.

2 Experimental

Nb single layers and $Nb/Pd_{1-x}Fe_x/Nb$ triple layers were grown in an ultra-high vacuum system (base pressure $\approx 5 \times 10^{-11}$ mbar) by e-beam evaporation onto *in situ* cleaned and annealed $Al_2O_3(11\bar{2}0)$ substrates at room temperature as described earlier [18]. During evaporation the background pressure was below 10^{-9} mbar. A set of eight samples with different d_{PdFe} was prepared during a single evaporation process. For the triple layers, a 200 Å film of Nb (purity 99.99%, Metallwerk Plansee, Reutte, Austria) was deposited first onto all substrates of one set with a evaporation rate of 0.5 Å/s. The thicknesses were measured with a quartz-crystal monitor. During the subsequent simultaneous evaporation of Pd (purity 99.95%, Goodfellow, Cambridge, England) and Fe (purity 99.998%, Goodfellow) from two different crucibles the computer-controlled sample shutter was opened stepwise to expose the samples one after another to the Pd and Fe beams. The evaporation rate of Pd was 0.25 Å/s and the Fe rate was adjusted to obtain the desired concentration x. Finally, a second 200 Å Nb layer was deposited on all samples. The relative error of the Fe concentration estimated from the variation of the evaporation rates during the process was less than 10%.

The growth of Pd on Nb and Nb on Pd was checked by reflection high-energy electron diffraction (RHEED). Diffraction patterns of the first Nb layer exhibit weak spots in addition to diffuse streaks very similar to previously reported patterns for the growth of Nb on Cu at room temperature [19]. This indicates an oriented growth of Nb (110) along the surface normal with limited order in the film plane and a rough surface due to the low adatom mobility. The pattern did hardly change with subsequent Pd deposition, where Pd is expected to grow on Nb (110) in the bulk fcc-structure along [111] for coverages larger than one monolayer ($d_{111} = 2.25$ Å) at room temperature with a lattice mismatch of 2–18% depending on the in-plane direction [20]. When the second Nb layer was deposited on Pd (111) the intensity of the diffuse spots increased which is characteristic for an enhanced surface roughness. These observations are consistent with the usual considerations of heteroepitaxial film growth between bcc (110) and fcc (111) surfaces taking into account the different surface energies γ of Nb ($\gamma = 2.98$ J/m^2) and Pd ($\gamma = 2.04$ J/m^2) [21,22], where layer-by-layer growth is expected for Pd on Nb in contrast to island growth for Nb on Pd if contributions due to misfit strains are neglected. Since the RHEED pattern did not change considerably upon deposition of Pd on Nb we conclude that Pd grows smoothly on the rough Nb (110) surface and is covered by the second 200 Å thick Nb film. In Nb/Pd and Nb/Fe multilayers interface roughnesses of 10 Å and 6 Å, respectively, were estimated from X-ray reflectivity measurements [13,19] indicating similar interface qualities in both systems. We therefore assume that for the case of $Pd_{1-x}Fe_x$ interlayers the growth behavior is independent of concentration x.

Symmetrical $\theta/2\theta$ scans were taken on some samples with a thick $Pd_{1-x}Fe_x$ interlayer ($d_{PdFe} > 30$ Å) using a standard X-ray powder diffractometer with Cu–K_α radiation. The scans indicate oriented growth of bcc-Nb (110) and fcc-PdFe (111) for $x \leq 0.4$ or bcc–Fe for $x = 1$ along the surface normal. The measured lattice parameters agree within 10% with data of 1000 Å rf-sputtered $Pd_{1-x}Fe_x$ films [24].

The electrical resistivity was measured in a He^4 cryostat with a conventional four-point probe using spring-loaded needles in magnetic fields up to 5 T. The superconducting critical temperature T_c was determined from the midpoint of the resistive transition. The transition width ΔT_c, estimated from the difference in temperature at 10% and 90% of the transition, was typically $\Delta T_c \leq 40$ mK for all samples. The upper critical magnetic field $B_{c2}(T)$ was determined from the midpoint of the transition measured by ramping up the magnetic field until 90% of the transition was accomplished and ramping down again. The temperature during this sweep was held constant within typically 2 mK. The critical-field transition width is defined as the field difference at 10% and 90% of the transition. The magnetic properties were investigated by SQUID magnetometry for temperatures 2–300 K and in magnetic fields up to 5 Tesla with the field oriented parallel to the sample surface.

Table 1. Magnetic properties of $Nb/Pd_{1-x}Fe_x/Nb$ triple layers.

x	d_{PdFe} (Å)	T_{Curie} (K)	μ_{exp} (μ_B)	μ_{exp}/μ_{bulk}	Ref.
0.05	18	60	0.17 ± 0.1	0.57 ± 0.3	this work
	∞	162	0.3	1	[25]
0.13	15	150	0.2 ± 0.1	0.3 ± 0.2	this work
	∞	320	0.66	1	[25]
0.20	9	70	0.13 ± 0.1	0.14 ± 0.1	this work
	12	175	0.1 ± 0.1	0.1 ± 0.1	this work
	17	> 300	0.96 ± 0.24	1.05 ± 0.4	this work
	∞	440	0.91	1	[25]

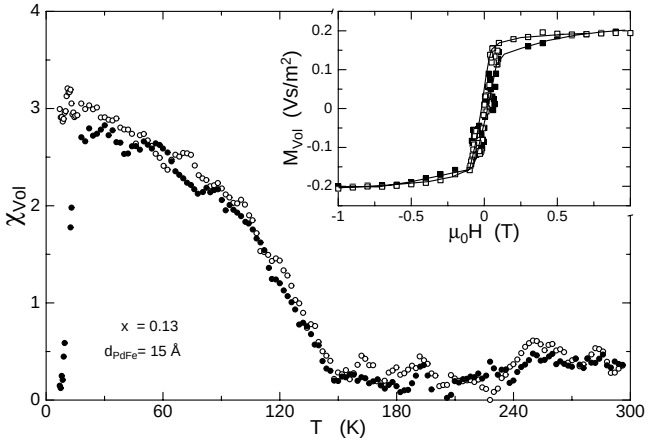

Fig. 1. Magnetic susceptibility χ *vs.* temperature T for $x = 0.13$ and $d_{PdFe} = 15$ Å measured in zero-field cooled (open circles) and field-cooled mode (closed circles). The applied magnetic field $B = \mu_0 H = 10$ mT was oriented parallel to the film plane. The inset shows a hysteresis loop $M(H)$ taken at $T = 8$ K (up sweep: solid symbols, down sweep: open symbols).

3 Results

3.1 Magnetic Properties

Figure 1 shows the dc-susceptibility $\chi(T)$ for one triple layer measured in the zero-field-cooled and field-cooled modes. The sharp decrease of the signal at low T is due to the superconducting transition at $T_c = 6.61$ K. The Curie temperature T_{Curie} was estimated from the extrapolation to $M(T \to T_{Curie}) = 0$. T_{Curie} is listed in Table 1 for some samples together with the values for bulk $Pd_{1-x}Fe_x$ alloys ($d_{PdFe} = \infty$). The ferromagnetic order was further checked on several samples of different concentration and $Pd_{1-x}Fe_x$ thickness by performing hysteresis loops $M(H)$ at $T = 8$ K, *i.e.* above T_c of these samples (Fig. 1, inset).

The magnetic properties of the films change with thickness and concentration. Table 1 clearly shows that T_{Curie} decreases with decreasing x when samples of almost equal d_{PdFe} are compared, as expected from the $T_{Curie}(x)$-dependence in the respective bulk alloys [15]. Furthermore, T_{Curie} decreases with decreasing d_{PdFe} for fixed concentration, *e.g.* $x = 0.20$. This is possibly due to finite-size effects where the thickness dependence of the Curie temperature is described by $T_{Curie} \propto d_F^{-\lambda}$ and the exponent λ depends on the dimensionality and universality class of the system.

For $x = 0.05$ the magnetic signal was very weak (not shown). From the susceptibility data a $T_{Curie} \approx 60$ K was estimated. For $x = 0.01$ a magnetic signal could not be detected. However, the magnetic behavior of these samples can be inferred from the investigation of the superconducting properties as will be discussed below.

The magnetic moment per atom μ_{exp} was determined from the saturation magnetization (Tab. 1), albeit with a large error for small d_{PdFe}. The average moment increases with concentration x for samples with roughly equal thickness, in accordance with the concentration dependence $\mu(x)$ in bulk alloys. However, the measured values are smaller than those of bulk samples ($\mu_{exp}/\mu_{bulk} < 1$, Tab. 1). On the one hand, this could be due to the existence of a magnetically "dead" layer at the $Pd_{1-x}Fe_x/Nb$ interface as reported previously for Nb/Fe multilayers [13,26]. In this case, the measured values can roughly be described by $\mu_{exp}/\mu_{bulk} = 1 - d_0/d$, where d_0 is the thickness of the nonmagnetic layer. From the data of Table 1 a thickness $d_0 \approx 8$ Å is estimated, *i.e.* 4 Å on either side of the $Pd_{1-x}Fe_x$ layer. This is comparable to the interface widths of 3.5–7 Å between Nb and pure Fe estimated from magnetization measurements on Nb/Fe multilayers [13,26]. On the other hand, the magnetization of the interlayer might also be influenced by effects of misfit strains or a change of the electronic structure at the two $Nb/Pd_{1-x}Fe_x$ interfaces. For the investigation of the magnetic properties of thin dilute $Pd_{1-x}Fe_x$ films the pure Pd might serve as a better substrate [27]. Hence, the existence of a magnetically "dead" layer at the $Nb/Pd_{1-x}Fe_x$ interface is presently unclear.

3.2 Upper critical magnetic field of Nb single films

Single Nb films with various thicknesses were investigated in order to check that the parallel critical field of $Nb/Pd_{1-x}Fe_x/Nb$ triple layers is not determined by the occurrence of surface superconductivity. Before presenting the results, we briefly summarize the usual behavior

of $B_{c2}(T)$ in dependence of the orientation of the magnetic field and of the dimensionality of the sample.

In general, the perpendicular critical magnetic field of superconducting films of thickness d obeys a linear temperature dependence, *i.e.* three-dimensional (3D) behavior, below T_c,

$$B_{c2\perp}(T) = \frac{\phi_0}{2\pi\xi_{0\parallel}^2}(1 - T/T_c) \quad (1)$$

because the sample dimensions are much larger than the temperature dependent Ginzburg-Landau coherence length parallel to the film plane, $\xi_\parallel(T) = \xi_{0\parallel}/\sqrt{1 - T/T_c}$, with $\xi_{0\parallel} = \xi_\parallel(T = 0)$.

In the parallel orientation, $B_{c2\parallel}(T)$ can be described by a similar expression where $\xi_{0\parallel}^2$ is replaced by $\xi_{0\parallel}\xi_{0\perp}$. Even in isotropic superconductors such as Nb, a difference in $\xi_{0\parallel}$ and $\xi_{0\perp}$ may occur because of an anisotropic microstructure. If just below T_c the perpendicular coherence length $\xi_\perp$ is larger than the thickness for very thin films, $\xi_\perp(T) \gg d$, the temperature dependence of $B_{c2\parallel}$ is described by the Tinkham expression for two-dimensional (2D) superconductors [28],

$$B_{c2\parallel}(T) = \frac{\sqrt{12}\phi_0}{2\pi\xi_{0\parallel}d}\sqrt{1 - T/T_c}. \quad (2)$$

Apart from a factor $\sqrt{12}/\pi$ the same result is obtained by using a Ginzburg-Landau approach for dirty and anisotropic superconductors, as has been done by Schneider and Locquet [29] to describe the overall temperature dependence of $B_{c2\parallel}(T)$.

At lower temperatures $\xi_\perp(T)$ can become smaller than the film thickness and the 3D behavior is recovered. Hence, because of the temperature dependence of $\xi(T)$ a dimensional crossover from 2D to 3D behavior should occur in $B_{c2\parallel}(T)$ with decreasing T. However, for sufficiently thick films this regime will not be entered due to the onset of surface superconductivity which occurs for $1.84\xi_\perp(T) < d$, *i.e.* when the diameter of a vortex $\approx 2\,\xi(T)$ is smaller than the film thickness [30]. In a field decreasing from well above $B_{c2\parallel}$, nucleation of superconducting regions will start near the surface leading to a superconducting sheath for fields $B_{c2\parallel} < B < B_{c3\parallel} = 1.69\,B_{c2\parallel}$ [31]. Generalizing this to anisotropic superconductors one obtains a linear behavior

$$B_{c3\parallel}(T) = \frac{1.69\phi_0}{2\pi\xi_{0\parallel}\xi_{0\perp}}(1 - T/T_c). \quad (3)$$

Therefore, in superconducting films a dimensional crossover from 2D (Eq. (2)) to surface superconductivity (Eq. (3)) can occur as a function of temperature and thickness in the parallel critical field.

Figure 2a shows the temperature dependence of $B_{c2\perp}$ for single films with different thickness d_{Nb} *vs.* the reduced transition temperature $t = T/T_c$. All films show a linear dependence for $t > 0.75$ characteristic for 3D behavior (Eq. (1)). For lower temperatures, the data points of films with $d_{Nb} \geq 275$ Å deviate from the linear dependence

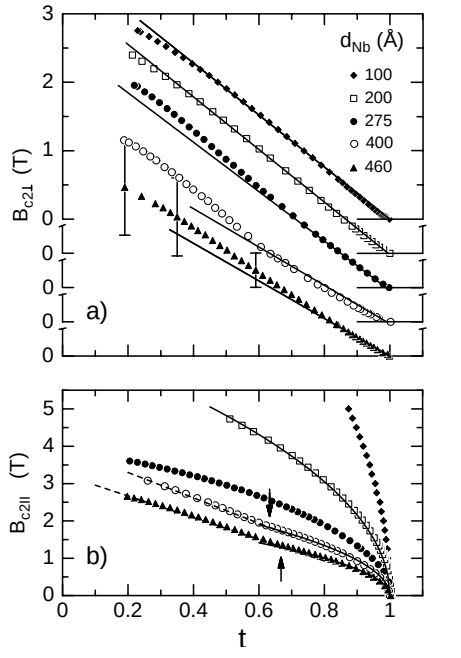

Fig. 2. (a) Perpendicular critical magnetic field $B_{c2\perp}$ *vs.* reduced temperature $t = T/T_c$ for Nb single films of different thickness. Solid lines indicate the linear temperature dependence near $t = 1$. The error bars do not exceed the symbol size for $t \geq 0.7$. (b) Parallel critical field $B_{c2\parallel}(t)$. Arrows indicate the temperature t^* below which surface superconductivity comes into play. Solid and dashed lines show the square-root and linear behavior above and below t^*, respectively.

with a concomitant increase in the transition width. ΔT_c is indicated by vertical bars. This behavior is presumably caused by thermally activated flux creep, which is more likely to occur in samples with a lower concentration of pinning centers. This is the case for thicker films which have a lower resistivity (Tab. 2), *i.e.* a lower concentration of defects.

The parallel critical field $B_{c2\parallel}(t)$ is shown in Figure 2b. For $t > 0.7$ all samples show a square-root dependence of $B_{c2\parallel}$, *i.e.* 2D behavior (Eq. (2)), indicating that $\xi_\perp(t)$ is larger than the thickness d_{Nb}. For films with $d_{Nb} \leq 275$ Å the 2D behavior survives down to the lowest temperature. In contrast, in thicker films with $d_{Nb} \geq 400$ Å, where below a certain temperature t^* the nucleation center moves from the center of the film to the surface, the temperature dependence of $B_{c2}(t)$ changes from square-root to linear behavior due to the onset of surface superconductivity.

The reduced perpendicular and parallel critical fields, *i.e.* $\epsilon = B_{c2\perp}(T)d^2\pi/2\phi_0$ and $h = B_{c2\parallel}(T)d^2\pi/2\phi_0$, are plotted in Figure 3 with T as an implicit parameter. For small h the data follow a single line $\epsilon = 0.33h^2$ in agreement with the theoretical prediction for the 2D regime according to Saint-James and de Gennes [31]. In films with $d \geq 400$ Å a change to a linear behavior due to the superconducting surface sheath is observed for $h > 2.2$, *e.g.* $\epsilon \approx 1.1h - 0.82$ for the 460 Å film. A behavior $\epsilon = (\xi_{0\perp}/1.695\,\xi_{0\parallel})h$ is expected when the anisotropy of

Table 2. Superconducting parameters of Nb films.

d_{Nb}	ρ ($\mu\Omega$cm)	l (Å)	ξ_0^ρ (Å)	$\xi_{0\parallel}$ (Å)	$\xi_{0\perp}$ (Å)	$\xi_{0\perp}/\xi_{0\parallel}$
100	15.35	24	79	90		
200	11.86	32	90	91		
275	8.0	47	107	93		
400	5.47	69	126	104	182	1.75
460	5.50	68	126	103	210	2.04

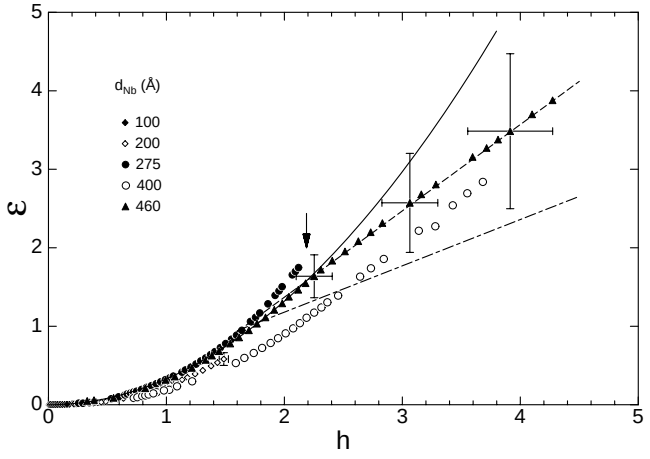

Fig. 3. Plot of the scaled perpendicular critical field $\epsilon = B_{c2\perp}(\pi d^2)/(2\phi_0)$ *vs.* the scaled parallel critical field $h = B_{c2\parallel}(\pi d^2)/(2\phi_0)$. Solid and dashed lines indicate the experimental behavior for the 460 Å film $\epsilon = 0.33h^2$ and $\epsilon = 1.1h - 0.82$, respectively. The transition takes place around $h \approx 2.2$ marked by arrow. Dashed-dotted line indicates $\epsilon = h/1.695$ without anisotropy ($\xi_{0\parallel} = \xi_{0\perp}$). Horizontal and vertical bars indicate the transition widths.

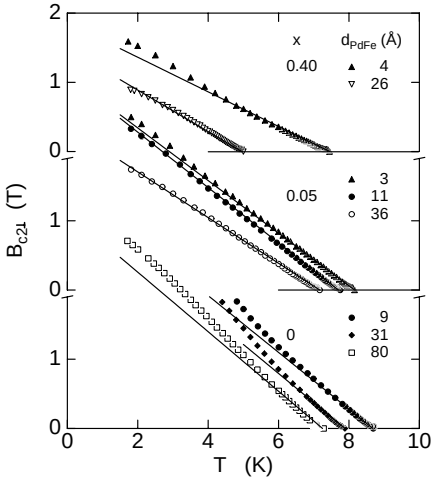

Fig. 4. Perpendicular critical magnetic field $B_{c2\perp}$ *vs.* temperature T for $Nb/Pd_{1-x}Fe_x/Nb$ triple layers of different thickness d_{PdFe} and concentration x. Solid lines indicate the linear temperature dependence near T_c.

the coherence length (Eqs. (1, 3)) is taken into account. The observed offset from a strict proportionality $\epsilon \propto h$ reflects the slightly superlinear t dependence of $B_{c2\perp}$. We neglect this fact for the following qualitative discussion. The crossover between the two regimes at $h \approx 2.2$ corresponds to the reduced temperature $t^* = T^*/T_c$ marked by arrows in Figure 2b. We obtain an anisotropy ratio $\xi_{0\perp}/\xi_{0\parallel}$ about 2 from the linear regime. With $\xi_{0\parallel}$ determined from $B_{c2\perp}$, the coherence length $\xi_{0\perp}$ can be derived (see Tab. 2). The fact that $\xi_{0\perp}$ is larger than $\xi_{0\parallel}$ can be explained by the anisotropic microstructure of the film, with columns perpendicular to the surface in addition to fine equiaxed grains, giving rise to an anisotropic electron diffusivity [32]. Alternatively, in the dirty limit an average coherence length ξ_0^ρ can be determined from electronic mean free path l [7], which was calculated from the residual resistivity ρ using $\rho l = 3.75 \times 10^{-16}\Omega\mathrm{m}^2$ [33]. It is reassuring that these values lie between the values of $\xi_{0\parallel}$ and $\xi_{0\perp}$ (see Tab. 2).

We conclude that for temperatures $T \geq 1.5$ K investigated here, Nb films with $d_{Nb} \leq 275$ Å show only 2D behavior in the parallel critical field without the occurrence of surface superconductivity, whereas in thicker films $B_{c2\parallel}(T)$ changes due to the onset of surface superconductivity. In this case, $\xi_{0\perp}$ can be measured. This is important for the following discussion of $Nb/Pd_{1-x}Fe_x/Nb$ triple layers with $d_{Nb} = 200$ Å. Moreover, we note that in $Nb/Pd_{1-x}Fe_x/Nb$ triple layers surface superconductivity is likely to occur only at even larger thicknesses due to the pairbreaking at the S/F interface.

3.3 Upper critical magnetic field of $Nb/Pd_{1-x}Fe_x/Nb$ triple layers

The perpendicular critical magnetic field for some selected samples of different d_{PdFe} and x is shown in Figure 4. In all cases, an almost linear T dependence suggesting 3D behavior is observed. Deviations at lower temperatures can be attributed to an increasing transition width in magnetic field which aggravates the precise determination of $B_{c2\perp}$. The temperature dependence of the parallel critical field $B_{c2\parallel}$ is shown in Figure 5. Two kinds of behavior are observed.

(1) For thin interlayer thickness and/or low iron concentration (including $x = 0$) $B_{c2\parallel}(T)$ exhibits a square-root like behavior close to T_c and a second square-root like behavior of different slope at lower temperatures.

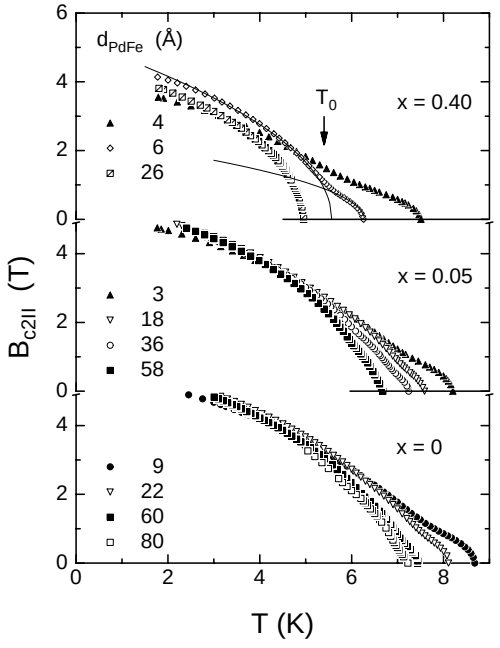

Fig. 5. Parallel critical magnetic field $B_{c2\parallel}$ *vs.* temperature T for $Pd_{1-x}Fe_x$ triple layers of different thickness d_{PdFe} and concentration x. For $x = 0.4$ and $d_{PdFe} = 6$ Å the solid lines indicate the different square-root behavior at temperatures below and above the 2D-2D crossover temperature T_0 marked by arrow.

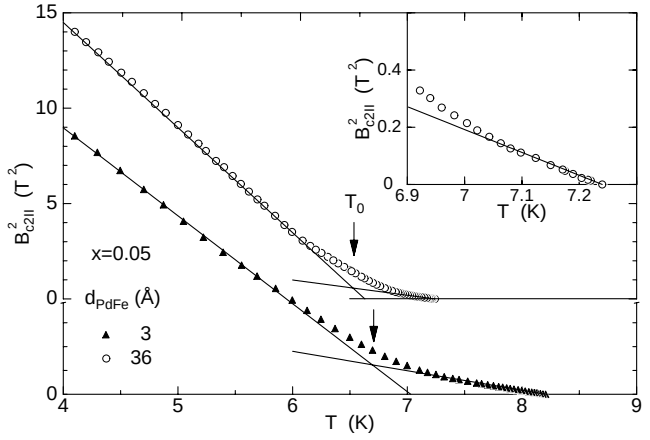

Fig. 6. $B^2_{c2\parallel}$ *vs.* T plot for two triple layers of different thickness d_{PdFe} with $x = 0.05$. Solid lines indicate the linear behavior in the two regimes. Arrows indicate the 2D-2D crossover temperature T_0. Inset shows the linear behavior near T_c for $d_{PdFe} = 36$ Å.

This is illustrated by way of example in Figure 6, where $B^2_{c2\parallel}$ plotted *vs.* T exhibits two linear regimes with a gradual transition around a temperature T_0 indicated by arrows. A change in the T dependence of $B_{c2\parallel}$ was also found in Pb/Ge multilayers with a limited number of bilayers and was attributed to a "2D-2D crossover" [34]. Roughly speaking, just below T_c both Nb layers are coupled through the interlayer, the order parameter extends over the total sample thickness and for $\xi_\perp(T) > d_{tot}$ a 2D behavior is observed (Eq. (2)). At lower temperatures and higher fields the Nb films are decoupled due to the suppression of superconductivity in the interlayer and the individual Nb layers give rise to a second 2D behavior in $B_{c2\parallel}$. The effect of an external magnetic field on the proximity effect was studied earlier in S/N junctions [35]. In the dirty limit the temperature dependence of the coherence length in the nonmagnetic metal N, $\xi_N = \sqrt{D/2\pi k_B T} \sim 1/\sqrt{T}$, would suggest that the coupling of the S layers increases with decreasing temperature. An increasing applied magnetic field has no effect on the overlap of both pair-amplitudes from S leaking into N with an exponential decay until superconductivity in N suddenly breaks down at the so-called break-down field B_0 [35]. At B_0 only a small superconducting sheath at the S/N interface survives, which further decreases in thickness with increasing B. The detailed behavior depends on the thickness d_N and on the transition temperature T_{cN} of the N layer. We simply adopt these results to the investigated S/F system, assuming that the exchange interaction in F increases the pairbreaking but does not change the qualitative behavior. For a strong ferromagnetic interlayer T_{cN} would be zero. Therefore, the data of samples with a thin and/or weakly ferromagnetic $Pd_{1-x}Fe_x$-layer can be explained in the following way: In low fields the Nb films are coupled and give rise to single-film behavior with $d_{tot} \approx 2d_{Nb} + d_{PdFe}$. When the break-down field B_0 is reached, superconductivity in the $Pd_{1-x}Fe_x$ layer is almost completely suppressed and the Nb layers decouple, showing a 2D behavior in $B_{c2\parallel}$. (More precisely, the transition in the (T, B) phase diagram (Fig. 6) occurs at a point where the $B_0(T)$ line crosses the $B_{c2\parallel}(T)$ curve.) This is further confirmed by the calculated coherence lengths $\xi_{0\parallel}$ (Eq. (2)) which agree well with those obtained from the $B_{c2\perp}(T)$ data if we assume $d = d_{tot}$ for coupled films ($T > T_0$) and $d = d_{Nb} = 200$ Å for decoupled films ($T < T_0$). The effective thickness of S might be somewhat smaller due to the proximity of the ferromagnetic material. This would lead to higher values of $\xi_{0\parallel}$ and better agreement with the values determined from the $B_{c2\perp}(T)$ behavior. We emphasize that the transition in $B_{c2\parallel}(T)$ from coupled to decoupled behavior appears at temperatures higher than $T^*/T_c \approx 0.6$ ($d = 400$ Å) below which the onset of surface superconductivity would change the $B_{c2\parallel}$ behavior as shown above.

(2) In samples with a large d_{PdFe} and/or large x the individual Nb layers are decoupled for all T by the strong pairbreaking of the magnetic interlayer. In this case a single square-root behavior of $B_{c2\parallel}(T)$ is observed down to the lowest temperature (*cf.* Fig. 5, $x = 0.40$, $d_{PdFe} = 26$ Å), similar to the case of a single 200 Å Nb film (Fig. 2b).

Hence, the characteristic temperature T_0 where the $B_{c2\parallel}(T)$ behavior changes depends on the interlayer thickness and the iron concentration. Figure 5 immediately shows that for constant x and increasing d_{PdFe}

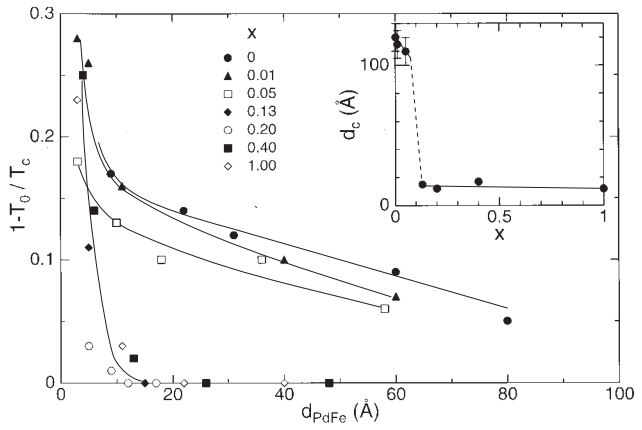

Fig. 7. Reduced characteristic temperature $(1 - T_0/T_c)$ *vs.* d_{PdFe} for different x. Solid lines serve as guide to the eye. Inset shows the critical thickness d_c derived from the intersection of $(1 - T_0/T_c)$ with the abscissa for different x.

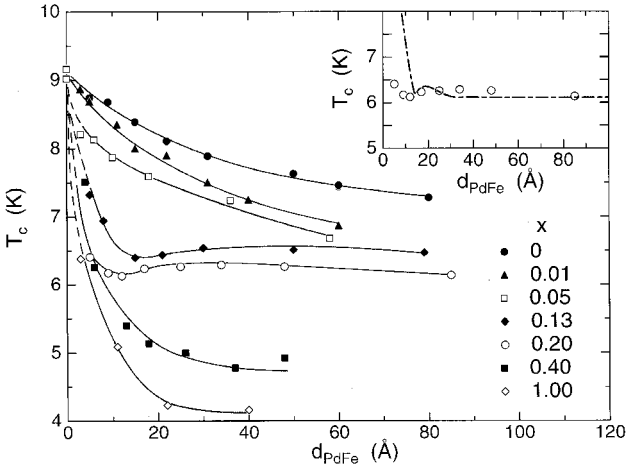

Fig. 8. Superconducting transition temperature T_c *vs.* interlayer thickness d_{PdFe} for different x. Solid lines serve as guide to the eye. Dashed lines show extrapolations to $T_c(d_{PdFe} = 0)$. The inset shows a fit by the theory of Radović *et al.* [2] (dashed-dotted line) to the data for $x = 0.20$, see text for further details.

the temperature T_0 shifts towards T_c which in turn decreases, until the individual Nb films are decoupled for all temperatures (*cf.* Fig. 5, $x = 0.40$). The $T_0(x, d_{PdFe})$ dependence is seen more clearly in Figure 7 where the reduced values $(1-T_0/T_c)$ are plotted *vs.* d_{PdFe} for different x. The data can be separated into two regimes. For small $x \leq 0.05$ a gradual decrease to large d_{PdFe} is seen. Moreover, for constant d_{PdFe} these samples show a systematic decrease of $(1 - T_0/T_c)$ with increasing x. In contrast, for $x \geq 0.13$ the data seem to follow a single line with a steep decrease to $(1 - T_0/T_c) = 0$ at small d_{PdFe}. (Note that for $d_{PdFe} \to 0$, T_0 should be zero for all x.) From the intersection of the data with the abscissa a critical thickness d_c can be determined in dependence of x. In samples with $x \leq 0.05$ this thickness was estimated by a linear extrapolation of the data. For each concentration, $d_c(x)$ is the smallest d_{PdFe} for which the transition from coupled to decoupled behavior is still observed whereas samples with $d_{PdFe} > d_c$ show a $B_{c2\parallel}(T)$ behavior of decoupled Nb films for all temperatures $T < T_c$. Thus, in samples with $d_{PdFe} = d_c$ the two pair amplitudes decaying from both S layers into the F layer do not overlap, *i.e.* $d_c/2 \approx (\mathrm{Re}\, k_F)^{-1} = \xi_F/2$ (Ref. [2]). Therefore, d_c can be identified as ξ_F as previously done by Koorevaar *et al.* for V/Fe multilayers [8].

The concentration dependence $d_c(x)$ is plotted in the inset. Again, the two different regimes can be identified. First, d_c decreases slightly with increasing x but becomes almost independent of x after a precipitous decrease between $x = 0.05$ and 0.13. Obviously, these two regimes are related to different pairbreaking mechanisms at the S/F interface, which will be discussed later. For the following discussion, we will take d_c as a measure of ξ_F whose concentration dependence is given by the inset of Figure 7 (as a "bulk" material parameter, ξ_F is assumed to be independent of d_{PdFe}).

3.4 Superconducting transition temperature of $Nb/Pd_{1-x}Fe_x/Nb$ triple layers

The superconducting transition temperatures T_c *vs.* interlayer thickness d_{PdFe} for sample sets of different x with constant $d_{Nb} = 200$ Å are shown in Figure 8. The transition width corresponds to the symbol size. For pure Pd ($x = 0$) a monotonic decrease of $T_c(d_{PdFe})$ from $T_c(0) = 9$ K is observed. Similar behavior has been reported recently for Nb/Pd multilayers with d_{Nb} which has been discussed in frame of the de Gennes-Werthamer theory [19].

With increasing x, the $T_c(d_{PdFe})$ curves are systematically lowered until for $x = 0.13$ and 0.20 a nonmonotonic behavior with a shallow minimum between $d_{PdFe} = 10{-}20$ Å is seen. For these sample sets, T_c becomes independent of the interlayer thickness for large d_{PdFe}. Note that for $x = 0.20$ all samples very likely have a ferromagnetic interlayer since already for $d_{PdFe} = 9$ Å a ferromagnetic hysteresis loop and a Curie temperature $T_{Curie} \approx 70$ K were measured (Tab. 1). Therefore, a nonmonotonic behavior caused by the establishment of long-range ferromagnetic order beyond a certain interlayer thickness, as observed in Fe/Nb/Fe triple layers [13], can be ruled out. The thickness where the minimum occurs for $x = 0.13$ and 0.20 is equal to the value of d_c determined from the critical-field behavior. This indicates that once the films are decoupled the transition temperature becomes independent of the thickness of the ferromagnetic interlayer. This has also been found in V/Fe multilayers [6,8]. For higher concentrations $x = 0.40$ and 1 this behavior does not change qualitatively although the shallow minimum is no longer present. We note that T_c still decreases for $d_{PdFe} \geq d_c$ although these samples are already completely decoupled. Besides the dependence of

$T_c(d_{PdFe})$ a general decrease of $T_c(x)$ with increasing x can be inferred when samples of nearly identical d_{PdFe} are compared.

For $x = 0.13$ and 0.20 a pronounced maximum of $T_c(d_{PdFe})$ at larger d_{PdFe} which would be attributed to a π-coupling mechanism as predicted by theory [2], is not observed. If such a mechanism does exist at all the absence of a T_c enhancement can have several reasons. First, the S/F coupling strength is an important parameter in the description of superconductivity in S/F systems. It is given by a parameter η which is related to the ratio of the respective conductivities $\eta = \sigma_F/\sigma_S$ where any spin-dependent scattering at the S/F interface is neglected. Applying the theory of Radović *et al.* [2,36] the overall $T_c(d_{PdFe})$ dependence for $x = 0.20$ can be described with $\xi_F = d_c \approx 12$ Å and the parameter $\epsilon = 10.5$ (Fig. 8, inset). (Since the theory is applied to S/F multilayers, where the superconducting layer is in proximity with a ferromagnetic layer at both boundaries, for the calculation d_S was taken $d_S = 2d_{Nb} = 400$ Å [7].) Using $\xi_S = 2\xi_0/\pi = 57$ Å we obtain $\eta = \xi_F/\epsilon\xi_S \approx 0.02$. Similar low values have also been reported for Nb/Gd [7,10] and Fe/Pb ($\eta = 0.04$) samples [14], where the values were found to be much smaller than the ones obtained from the conductivity ratio. For the Nb/Gd system, the different obtained parameters $\eta = 0.047$ for evaporated samples [7] and $\eta = 0.013$ for sputtered samples [10] indicate a strong influence of the preparation method on η. Second, the interface transparency for conduction electrons can be reduced because of intrinsic reasons, like the splitting of the ferromagnetic conduction band. Third, the nonmonotonic behavior is completely suppressed if the spin-orbit scattering is strong compared to the ferromagnetic exchange interaction [4,14].

We conclude that from T_c measurements alone and the absence of a $T_c(d_F)$ oscillation it is not possible to prove or dismiss the existence of a π-coupling mechanism. Additional experiments on, for instance, S/F/S Josephson junctions have to be performed in the future to look for unequivocal evidence for such a phenomenon.

4 Discussion

Obviously, the concentration dependence of the critical-field behavior and of the transition temperature can be separated into two different scenarios. For low concentrations $x \leq 0.05$ the reduced characteristic temperature $(1-T_0/T_c)$ as well as T_c gradually decrease with increasing d_{PdFe}. For these samples the critical thickness d_c is large ($d_c \approx 100$ Å) and the individual Nb layers are coupled *via* the $Pd_{1-x}Fe_x$ interlayer. From the magnetic measurements it is not possible to decide unambiguously whether the small-d_{PdFe} samples with $x < 0.05$ exhibit long-range ferromagnetic order.

In contrast, for $x \geq 0.13$ the magnetic measurements show definitely that the interlayer is ferromagnetically ordered. In this case a clear transition from coupled to decoupled behavior in $B_{c2\parallel}(T)$, where T_c becomes independent of d_{PdFe}, is found at $d_c \approx 12$ Å. This transition allows an experimental determination of the characteristic penetration depth of Cooper pairs in the ferromagnetic layer, ξ_F, a quantity that is usually not accessible in experiment. In the theory of Radović *et al.* [2] the minimum of the $T_c(d_{PdFe})$ curve appears around $d_F \approx \xi_F$. Therefore, the critical-field measurements may serve as an independent method for the determination of ξ_F.

First, we consider the two extreme cases of a pure Fe interlayer ($x = 1$) and a pure Pd interlayer ($x = 0$). For a pure Fe interlayer we can calculate the parameter $I = 4\hbar D_F/\xi_F^2$ from the measured $\xi_F \approx 12$ Å. For the estimation of $D_F = v_F l/3 = 2.7$ cm^2/s we take $l \approx \xi_F$ as the electronic mean free path and a Fermi velocity $v_F^{Fe} = 6.9 \times 10^7$ cm/s for *sp* electrons [37]. This yields $I \approx 0.5$ eV as a lower limit in fair agreement with $I \approx 1$ eV for bulk iron. For a pure Pd interlayer, which is presumably not in a ferromagnetic state, at least not for $T > 1.5$ K, the application of the theory is questionable. An upper limit of $I \approx 80$ meV can be estimated as before, which is unrealistically low, even for the $4d-4d$ exchange interaction in pure Pd. However, spin fluctuations or "paramagnons" with a characteristic energy of $E = 21$ meV are possibly pairbreaking in Pd [38]. Moreover, tunneling experiments on Pd–Pb sandwiches have shown that Pd is not gapless down to a thickness of 500 Å which indicates that the pairbreaking is much weaker than by magnetic impurities and in magnetic fields [39] thus leading to a large ξ_F. Hence, for the extreme cases of $x = 0$ and $x = 1$ the experimentally determined values of ξ_F can be reasonably explained by pairbreaking due to the presence of spin fluctuations and by the exchange interaction, respectively.

Concerning the samples with an alloy interlayer the interesting point is that d_c, *i.e.* ξ_F, is more or less independent of concentration for $0.13 \leq x \leq 1$. Band-structure calculations of ordered fcc Fe–Pd alloys show that the average exchange splitting decreases by no more than a factor of two when the Fe content is successively reduced from Fe_3Pd to $FePd_3$ [23]. The decrease is basically due to the weaker $4d-4d$ exchange interaction compared to the $3d-3d$ interaction. Furthermore, the Fermi velocity of Pd is smaller than of Fe, $v_F^{Pd} = 2 \times 10^7$ cm/s [39]. This suggests that with decreasing x the accompanying decrease of I is more or less compensated by a decrease of D_F. Besides, ξ_F depends only weakly on D_F/I, *viz.* $\propto \sqrt{D_F/I}$. This explains why $d_c \approx$ constant for $0.13 \leq x \leq 1$.

For low concentrations $x < 0.05$ the critical thickness is much larger. Since in this regime the interlayer is likely to be in the paramagnetic state the reduction of T_c is presumably due to the well-known pairbreaking caused by spin-flip scattering first investigated in the classical work by Hauser *et al.* [40]. This is further corroborated by the gradual increase of ξ_F with decreasing x (Fig. 7). Hence, the large change of ξ_F around $x \approx 0.1$ marks the transition from a paramagnetic to a ferromagnetic interlayer, similar to the previous reports on Nb/Gd [7] and Nb/Fe systems [13] where such a behavior was found in dependence of the thickness of the F layer. This large

difference between ξ_F in both regimes demonstrates that the pairbreaking by the exchange interaction is much stronger than by spin-flip scattering.

Samples with $x = 0.05$ seem to show a contradictory behavior, *i.e.* a weak ferromagnetic signal for $d_{PdFe} = 18$ Å with a strong reduction of the Curie temperature and a large $d_c \approx 100$ Å together with a gradual decrease of $T_c(d_{PdFe})$. Note that for $d_{PdFe} = 18$ Å the saturation magnetization was measured at $T = 8$ K slightly above T_c. Therefore, a possible explanation for the "paramagnetic-like" behavior inferred from the superconducting results might be a destruction of the long-range ferromagnetic order by the onset of superconductivity. A decrease of the effective magnetization of the ferromagnetic interlayer below the superconducting critical temperature of the Nb layer has been reported recently for Nb/Fe bilayers [41]. Although some evidence for a new cryptoferromagnetic state in the F layer has been given, the microscopic mechanism is not clear. In the present case more detailed magnetic measurements above and below T_c would be desirable but are difficult to perform due to the very weak magnetic signal of the diluted samples.

However, the concentration dependence of d_c extracted from the superconducting measurements can be considered as a magnetic response, although the magnetic properties of very diluted samples could not be measured directly. Another approach has been reported for $V/V_{1-x}Fe_x$ multilayers, where the effect of the exchange field on the interface transparency for Cooper pairs, was investigated by $T_c(d_S, x)$ measurements [42].

5 Conclusion

The occurrence of a transition from coupled to decoupled behavior in the parallel critical field of $Nb/Pd_{1-x}Fe_x/Nb$ triple layers allows a determination of the characteristic penetration depth of Cooper pairs ξ_F in the F layer. With increasing x, this length changes abruptly in a small concentration interval due to a transition from a paramagnetic to a ferromagnetic interlayer leading to a change in the underlying pairbreaking mechanism while it is found to be more or less independent of x in the ferromagnetic regime. It is reassuring that the strong difference in ξ_F between $x = 0.05$ and 0.13 is reflected in the different $T_c(d_{PdFe})$ behavior. Although the present work presents a step forward in identifying the requirements for possible π-junctions in S/F layers or multilayers, a decisive experimental test for this possibility must await phase sensitive measurements such as the Josephson effect.

We thank M. Kelemen for performing the SQUID measurements, H. Claus for several discussions, and L.R. Tagirov for helpful remarks. This work was partly supported by the Deutsche Forschungsgemeinschaft through Graduiertenkolleg "Kollektive Phänomene im Festkörper".

References

1. A.I. Buzdin, M.Yu. Kupriyanov, JETP Lett. **52**, 487 (1990).
2. Z. Radović, M. Ledvij, L. Dobrosavljević-Grujić, A.I. Buzdin, J.R. Clem, Phys. Rev. B **44**, 759 (1991).
3. L.N. Bulaevskiĭ, V.V. Kuziĭ, A.A. Sobyanin, JETP Lett. **25**, 290 (1977).
4. E.A. Demler, G.B. Arnold, M.R. Beasley, Phys. Rev. B **55**, 15174 (1997).
5. M.G.T. Khusainov, Yu.N. Proshin, Phys. Rev. B **56**, R14 283 (1997); L.R. Tagirov, Physica C 307, 145 (1998).
6. H.K. Wong, B.Y. Jing, H.Q. Wang, J.B. Ketterson, J.E. Hilliard, J. Low. Temp. Phys. **63**, 307 (1986).
7. C. Strunk, C. Sürgers, U. Paschen, H.v. Löhneysen, Phys. Rev. B **49**, 4053 (1994).
8. P. Koorevaar, Y. Suzuki, R. Coehoorn, J. Aarts, Phys. Rev. B **49**, 441 (1994).
9. P. Koorevaar, R. Coehoorn, J. Aarts, Physica C **248**, 61 (1995).
10. J.S. Jiang, D. Davidović, D.H. Reich, C.L. Chien, Phys. Rev. Lett. **74**, 314 (1995).
11. J.S. Jiang, D. Davidović, D.H. Reich, C.L. Chien, Phys. Rev. B **54**, 6119 (1996).
12. L.V. Mercaldo, C. Attanasio, C. Coccorese, L. Maritato, S.L. Prischepa, M. Salvato, Phys. Rev. B **53**, 14040 (1996).
13. Th. Mühge, N.N Garif'yanov, Yu.V. Goryunov, G.G. Khaliullin, L.R. Tagirov, K. Westerholt, I.A. Garifullin, H. Zabel, Phys. Rev. Lett. **77**, 1857 (1996).
14. N.N Garif'yanov, Yu.V. Goryunov, Th. Mühge, L. Lazar, G.G. Khaliullin, K. Westerholt, I.A. Garifullin, H. Zabel, Eur. Phys. J. B **1**, 405 (1998).
15. G.J. Nieuwenhuys, Adv. Phys. **24**, 515 (1975) and references therein.
16. T. Hermannsdörfer, S. Rehmann, W. Wendler, F. Pobell, J. Low Temp. Phys. **104**, 49 (1996).
17. C. Büscher, T. Auerswald, E. Scheer, A. Schröder, H.v. Löhneysen, H. Claus, Phys. Rev. B **46**, 983 (1992).
18. C. Sürgers, H.v. Löhneysen, Thin Sol. Films **219**, 69 (1992).
19. S. Kaneko, U. Hiller, J.M. Slaughter, C.M. Falco, C. Coccorese, L. Maritato, Phys. Rev. B **58**, 8229 (1998).
20. B.C. Bolding, E.A. Carter, Phys. Rev. B **44**, 3251 (1991) and references therein.
21. E. Bauer, J.H. van der Merwe, Phys. Rev. B **33**, 3657 (1986).
22. L.Z. Mezey, J. Giber, Jpn J. Appl. Phys. **21**, 1569 (1982).
23. P. Mohn, E. Supanetz, K. Schwarz, Aust. J. Phys. **46**, 651 (1993).
24. S.L. Zhang, K. Sumiyama, Y. Nakamura, J. Magn. Magn. Mater. **73**, 58 (1988).
25. J. Crangle, Philos. Mag. **5**, 335 (1960).
26. J.E. Mattson, C.H. Sowers, A. Berger, S.D. Bader, Phys. Rev. Lett. **68**, 3252 (1992).

27. D.J. Webb, J.D. McKinley, Phys. Rev. Lett. **70**, 509 (1993).
28. M. Tinkham, *Introduction to Superconductivity* (McGraw-Hill, New York, 1975).
29. T. Schneider, J.-P. Locquet, Physica C **179**, 125 (1991).
30. H.J. Fink, Phys. Rev. **177**, 732 (1969).
31. D. Saint-James, P.G. de Gennes, Phys. Lett. **7**, 306 (1963).
32. C. Sürgers, C. Strunk, H.v. Löhneysen, Thin Sol. Films **239**, 51 (1994).
33. H.W. Weber, F. Seidl, C. Laa, E. Schachinger, M. Prohammer, A. Junod, D. Eckert, Phys. Rev. B **44**, 7585 (1991).
34. D. Neerinck, K. Temst, C. van Haesendonck, Y. Bruynseraede, A. Gilabert, I.K. Schuller, Phys. Rev. B **43**, 8676 (1991).
35. Orsay Group on Superconductivity, Phys. Kondens. Materie **6**, 307 (1967).
36. A.I. Buzdin, B. Bujicic, M.Yu. Kupriyanov, Sov. Phys. JETP **74**, 124 (1992).
37. M. Yousouf, P.Ch. Sahn, K.G. Rajan, Phys. Rev. B **34**, 8086 (1986).
38. H.G. Zarate, J.P. Carbotte, Phys. Rev. B **35**, 3256 (1987) and references therein.
39. L. Dumoulin, P. Nedellec, P.M. Chaikin, Phys. Rev. Lett. **47**, 208 (1981).
40. J.J. Hauser, H.C. Theuerer, N.R. Werthamer, Phys. Rev. **142**, 118 (1966).
41. Th. Mühge, N.N Garif'yanov, Yu.V. Goryunov, K. Theis-Bröhl, K. Westerholt, I.A. Garifullin, H. Zabel, Physica C **296**, 325 (1998).
42. J. Aarts, J.M.E. Geers, E. Brück, A.A. Golubov, R. Coehoorn, Phys. Rev. B **56**, 2779 (1997).